https://doi.org/10.5194/egusphere-2023-540
Preprint. Discussion started: 23 August 2023

Investigating the contribution of grown new particles to cloud condensation nuclei with largely varying pre-existing particles - Part 2: Modeling chemical drivers and 3-D NPF occurrence

Ming Chu[1], Xing Wei[1], Shangfei Hai[2], Yang Gao[1,3], Huiwang Gao[1,3], Yujiao Zhu[4], Biwu Chu[5], Nan Ma[6], Juan Hong[6], Yele Sun[7], Xiaohong Yao[1,3]

[1]Frontiers Sci Ctr Deep Ocean Multispheres & Earth, Key Laboratory of Marine Environment and Ecology (MoE) and Sanya Oceanographic Institution, Ocean University of China, Qingdao, China

[2] College of Oceanic and Atmospheric Sciences, Ocean University of China, Qingdao 266100, China

[3] Laboratory for Marine Ecology and Environmental Sciences, Qingdao National Laboratory for Marine Science and Technology, Qingdao, China

[4]Environment Research Institute, Shandong University, Qingdao 266237, China

[5]State Key Joint Laboratory of Environment Simulation and Pollution Control, Research Center for Eco-Environmental Sciences, Chinese Academy of Sciences, Beijing 100085, China

[6]Institute for Environmental and Climate Research, Jinan University, Guangzhou, 510000, China

[7]State Key Laboratory of Atmospheric Boundary Layer Physics and Atmospheric Chemistry, Institute of Atmospheric Physics, Chinese Academy of Sciences, Beijing, 100029, China

Correspondence to: Yang Gao (yanggao@ouc.edu.cn) and Xiaohong Yao (xhyao@ouc.edu.cn)

Abstract. In this study, we utilized a 20-bin WRF-Chem (Weather Research and Forecast coupled with Chemistry regional model) to investigate the contributions of chemical drivers to the growth of newly formed particles, as well as to simulate the three-dimensional dynamics of new particle formation (NPF) events over the North China Plain during a summer campaign in 2019, which was reported in the accompanying paper. The model demonstrated good performance in replicating the occurrence of NPF, the growth pattern of newly formed particles, and the number concentration of particles in the size range of 10–40 nm in five events between June 29 and July 6. This period was characterized by a high frequency of NPF occurrence (>60 %). During this time, the model was also able to accurately reproduce the levels of organics in $PM_{1.0}$ relative to observations, and to reasonably replicate the levels of SO_4^{2-} and NH_4^+ in $PM_{1.0}$, as well as $PM_{2.5}$ mass concentrations. Therefore, we further analyzed three NPF events with distinct particle growth characteristics: Case 1, featuring observable growth of newly formed particles to cloud condensation nuclei (CCN) size on July 1–2; Case 2, characterized by continuous growth of new particles for several hours without any net contribution to CCN on July 3; and Case 3, where no detectable continuous growth of newly formed particles was observed on July 6. In these instances, the model tended to overpredict the condensation of H_2SO_4 vapor during daytime and the formation of NH_4NO_3 during nighttime, resulting in an overestimation of the hygroscopicity parameter of nanometer particles. Nevertheless, the model was able to reasonably reproduce the CCN (cloud condensation nuclei) at a super saturation (SS) of 0.4 % on days with NPF, compared to the observations. This was because the overestimation effect caused by inorganics was offset by the model's underestimation of CCN originating

https://doi.org/10.5194/egusphere-2023-540
Preprint. Discussion started: 23 August 2023

from submicron-sized particles. Additionally, three-dimensional simulations of NPF events have demonstrated some key findings. Firstly, NPF consistently initiates at the upper fraction of the planetary boundary layer (PBL) before expanding. Secondly, during daytime growth of newly formed particles in the PBL, organics play a dominant role, whereas the primary chemical drivers shift to inorganic species in the free troposphere. However, to confirm these findings, vertical observations are required.

Keywords: NPF; WRF-Chem; secondary organic aerosols; NH_4NO_3; spatial inhomogeneity

1 Introduction

In the atmosphere, gaseous precursors come together to form a critical nucleus, which is then followed by the growth of newly nucleated particles. This process is known as new particle formation (NPF) events and has been extensively studied (Kulmala et al., 2004; Bzdek and Johnston, 2010; Zhang et al., 2012). NPF events cause a sharp increase in particle number concentrations (PNCs) and can potentially impact the global climate by acting as cloud condensation nuclei (CCN) (Huang et al., 2016; Gordon et al., 2017; Yu et al., 2017). Specifically, NPF has been estimated to contribute as much as 45 % to the global budget of cloud condensation nuclei (CCN) (Spracklen et al., 2008; Merikanto et al., 2009; Williamson et al., 2019). Furthermore, newly formed particles resulting from NPF have been shown to continue growing for several days, making a substantial contribution to atmospheric particle mass concentrations. This link between NPF and subsequent haze events has been observed in China (Zhang et al., 2012; Chu et al., 2021; Kulmala et al., 2022). In fact, if the newly formed particles grow to a sufficient size, they may have direct climate effects by altering atmospheric radiation.

The North China Plain (NCP) is one of the largest plains in Asia, but suffers from air pollution to some extent (Li et al., 2017; Jiang and Bai, 2018; Ma et al., 2019; Yang et al., 2021). Despite this, the NCP frequently experiences NPF events, due to the abundance of precursors such as sulfuric acid, ammonia, amines, and secondary gaseous organics, as well as dry weather conditions (Wehner et al., 2004; Wu et al., 2007; Yue et al., 2010; Wang et al., 2015; Zhu et al., 2017; Ma et al., 2021; Chu et al., 2021). It is worth noting that there has been a significant decrease in air pollutant emissions, including SO_2 and NO_x, in the NCP over the past decade, as reported by Chen et al. (2019a), Wen et al. (2021), and Zhu et al. (2021a). This decrease may theoretically lower the probability of newly formed particles growing to the CCN required size, as suggested by previous studies (Dusek et al., 2006; Hudson, 2007; Zhu et al., 2021b). After considering the situation outlined above, it is imperative and essential to conduct an updated study that quantifies the diverse contributions of chemical drivers in NPF events over NCP.

Commercial particle sizers, such as the Scanning Mobility Particle Sizer (SMPS), Wide-range Particle Sizer (WPS), and fast mobility particle sizer (FMPS) have limitations in detecting particles smaller than 3 or 5.6 nm and have low detection efficiency for particles smaller than 15 nm. As a result, newly formed particles are typically observed at initial sizes larger than 6–15 nm using these particle sizers. The growth of clusters to larger than 6–15 nm takes hours, during which time NPF can occur and move with the air mass. The use of one fixed-site to observe condensable vapors is not sufficient to explain NPF occurring downwind, and it is difficult to perform Lagrange observations with moving air

https://doi.org/10.5194/egusphere-2023-540
Preprint. Discussion started: 23 August 2023

masses. Thus, three-dimensional (3-D) modeling studies are needed to determine where NPF events initially occur. Furthermore, it has been suggested that long-duration NPF events can extend to hundreds of kilometers in the horizontal direction (Wehner et al., 2007; Hussein et al., 2009; Crippa and Pryor, 2013; Pikridas et al., 2015; Kerminen et al., 2018). However, relying solely on data from one or two observation sites limits our understanding of the spatial inhomogeneity of NPF events at a regional scale. Factors such as NPF event duration, particle formation, and particle growth rates can differ significantly therein (Kim et al., 2016; Dai et al., 2017; Shen et al., 2018). Therefore, NPF modeling studies are critical to fully explore the 3-D dynamic evolution of NPF events.

In the literature, Matsui et al. (2009) utilized the Weather Research and Forecasting (WRF)-Community Multiscale Air Quality (CMAQ) and WRF-Chem models to reasonably replicate PNCs and identify instances of NPF during the CARE-Beijing 2006 campaign. Similarly, Chen et al. (2014) implemented a few simulations of PNCs in NCP using the Nested Air Quality Prediction Modeling System (NAQPMS) with an Advanced Particle Microphysics (APM) (Chen et al., 2017; 2019b). The NPF-explicit WRF-Chem model has reportedly demonstrated a good performance in simulating some regional NPF events in East Asia and North America (Matsui et al., 2013; Dong et al., 2019; Yu et al., 2020), and Lai et al. (2022) investigated the vertical transport and distribution of particles using the WRF-Chem model. Therefore, it would be beneficial to utilize this model to examine the recently observed NPF events in NCP, particularly in terms of their 3-D evolution and chemical drivers in growing newly formed particles in the horizontal and vertical directions, as highlighted in the companion paper, which discusses the low probability of newly formed particles growing to the required size for CCN formation. It is important to note, however, that there may be significant uncertainties in PNC emission factors and particle number size distributions (PNSD) from primary sources in China due to the lack of such data (Yao et al., 2005; Shen et al., 2022).

In this study, the NPF-explicit WRF-Chem model is used to investigate NPF events observed at a mountain site in NCP from June 23 to July 14, 2019, in terms of chemical drivers to grow newly formed particles to CCN size, the uncertainty of estimated contributions of grown new particles to CCN loadings, and 3-D occurrence of NPF events. Before the result presentation and discussion, a comprehensive model performance evaluation will be delivered in Section 2.4. Section 3.1 will provide an overview of modeling NPF events. The simulated chemical drivers to grow newly formed particles at the ground level and different heights will be presented in Sections 3.2 and 3.3, respectively. Section 3.4 will analyze 3-D occurrence of NPF events and transport of newly formed particles. Section 3.5 will address what happened for grown new particles after their signals disappearing from observations.

2 Methods

2.1 Observational information

The Beijing Forest Ecosystem Positioning Research Station is situated at an altitude of 1170 m above sea level (a.s.l.) and is surrounded by Yanshan mountain (39.96°N, 115.43°E; hereinafter referred to as the mountain station). The area is mainly covered by secondary forest vegetation, such as secondary shrub, oak, and birch forest. The mountain station is located in the western edge of Beijing (see Fig. 1)

https://doi.org/10.5194/egusphere-2023-540
Preprint. Discussion started: 23 August 2023

and is far from industrial and urban areas. Strong air pollutant emission sources and heavily polluted cities are distributed in the southwest direction, about 200–500 km away from the site (Ma et al., 2019). On the other hand, no strong air pollutant emission sources are found in the north direction where the play fields of the 2022 Beijing Olympic Winter Games are located. The simulated NPF events in the north direction were significantly stronger than those in other zones, as will be explained later.

The performance of the model was assessed using a suite of observational data, which were detailed in the companion paper. These included both on-line and off-line measurements of total PNCs, PNSD, and CCN, which were conducted using a condensation particle counter (CPC; TSI Model 3775), a fast mobility particle sizer (FMPS, TSI Model 3091), a scanning mobility particle sizer (SMPS, Grimm), and a continuous flow CCN counter (CCNC, DMT Model 100), respectively. The instruments were located on the third floor of the main station building. In addition, a high-volume TSP sampler was used for off-line sampling to analyze water-soluble ions, as well as organic and elemental carbon, during the period. For measurements taken between June 14 and 30, 2019, a combination of the SMPS and the CPC was used. The FMPS was prepared for measurements between June 23 and July 14, 2019, with a one-week overlap with SMPS measurements. During laboratory tests conducted after the campaign, it was observed that the dryer caused significant particle diffusion losses when the SMPS and CPC were used with flow rates less than 1 L min^{-1}. However, the FMPS with a flow rate of 10 L min^{-1} did not suffer from this issue and was able to accurately capture rapid changes in PNCs from primary and secondary sources, as documented in previous studies (Yao et al., 2005; 2006; Man et al., 2015). Therefore, only the data collected between June 23 and July 14 were used for evaluation. It is worth noting that the PNSDs were employed for a comparative analysis of NPF events with those measured at an urban site in Beijing, as presented in Zhou et al. (2020).

2.2 NPF-explicit WRF-Chem Model

The NPF-explicit WRF-Chem model (Grell et al., 2005; Fast et al., 2006) was employed to simulate the occurrence of NPF events in the NCP during the period from June 23 to July 14, 2019. The model was equipped with a 20-bin MOSAIC module that covered particle diameters ranging from 1 nm to 10 μm (Matsui et al., 2011; Matsui et al., 2013; Lupascu et al., 2015; Lai et al., 2022). The parameter settings used in the model are shown in Table S1. It should be noted that the anthropogenic emissions in China for the year 2019 were not publicly available. Therefore, custom-modified MEIC_2019 emissions, which were based on MEIC_2016 and assumed a linear downward trend in the total amounts of chemicals from 2016 to 2019, were used in the modeling. The custom-modified MEIC_2019 emissions were successfully applied to simulate $PM_{2.5}$ in the NCP, and more information can be found in Zhang et al. (2022).

2.3 Selection of nucleation mechanism

Based on previous research on the importance of H_2SO_4 and organic vapors in modeling high-altitude NPF events, as well as the varied environmental conditions found in forest stations (Metzger et al., 2010; Schobesberger et al., 2013; Riccobono et al., 2014; Yu and Hallar, 2014; Bianchi et al., 2016; Dong et al., 2019), this study has selected the empirical H_2SO_4-organic nucleation mechanism in the NPF-explicit WRF-Chem model for simulating NPF events. The mechanism can be expressed as:

https://doi.org/10.5194/egusphere-2023-540
Preprint. Discussion started: 23 August 2023

$$J = K_{ORG} \times [H_2SO_4] \times [NucORG] \quad (1)$$

The variable J represents the rate of formation of activated clusters with a diameter of 1 nm (measured in cm^{-3} s^{-1}). K_{ORG} (measured in cm^{-3} s^{-1}) is an empirical coefficient for nucleation, while $[H_2SO_4]$ and [NucORG] represent the concentrations of gaseous sulfuric acid (measured in cm^{-3}) and low-volatility organic compounds (measured in cm^{-3}), respectively (Lupascu et al., 2015). The nucleation empirical coefficient is a key parameter in accurately simulating new particle formation events, but its value can vary significantly between different atmospheric conditions (Sihto et al., 2006; Riipinen et al., 2007; Matsui et al., 2011; Cui et al., 2014; Sullivan et al., 2018). In this study, a series of sensitivity tests were conducted to identify the optimal value of K_{ORG} for modeling NPF events in the NCP. The results showed that a value of K_{ORG} = 6.2 $\times 10^{-18}$ produced the best performance, and was therefore used to replace the default value of K_{ORG} =1.00 $\times 10^{-15}$ for modeling purposes.

2.4 Model performance evaluation

To evaluate the performance of the model, we compared the modeled PNCs, mass concentrations of secondary ions, and $PM_{2.5}$ mass concentrations with the observations. Specifically, we evaluated the modeled CN_{10-40}, which is the summed PNC in the range of 10–40 nm, by comparing it with the observations (Fig. 2a). The simulated CN_{10-40} showed good agreement with the observations during the period from June 29 to July 6 (unshaded area in Fig. 2a), but not before June 29 and after July 6. To quantify the simulation performance of the CN_{10-40}, we used three statistical parameters: mean fractional bias (MFB), mean fractional error (MFE), and correlation coefficient (R) (Fig. 2b–d). During the NPF events period, the MFB of 24 % and the MFE of 66 % on June 29–July 6 met the benchmarks (MFB: 50 %; MFE: 75 %, US EPA, 2007). The correlation coefficient was 0.61, which ranked among the upper values of 0.4–0.7 reported in the literature (Matsui et al., 2013; Lupascu et al., 2015; Dong et al., 2019). However, the three parameters showed poor performance when the model reproduced the observations before June 29 and after July 6. The reasons for the poor simulation performance are yet to be explained. In our unpublished study, we try to modify the model and improve the poor simulation performance in the coastal atmosphere. The modifications are not applicable for this study and are thereby not applied.

The simulated mass concentrations of SO_4^{2-} in PM_{10}, shown in Fig. 3a–e, were found to reasonably reproduce the observations in the total suspended particles collected at the mountain station, with MFB = -28 %, MFE = 41 %, and R = 0.69. However, the model tended to overestimate the mass concentrations of organics (ORG in Fig. 3b), NO_3^-, and NH_4^+ in PM_{10} before June 29 and after July 6. Despite this, the model was able to reproduce low mass concentrations of all three species in PM_{10} between June 29 and July 6. It should be noted that the poor performance in reproducing the observed organics, NO_3^-, and NH_4^+ could also be partially attributed to sampling artifacts, given their higher volatility compared to ammoniated sulfate acid (Yao et al., 2002; Chow et al., 2010).

During this study period, the chemical composition measured by the ToF-ACSM in Beijing (39.98ºN, 116.39ºE) was used for evaluation. The simulated mass concentrations of SO_4^{2-}, NO_3^-, NH_4^+, and organics in $PM_{1.0}$ were reasonably consistent with the observations from June 29 to July 6, which had frequent NPF events (unshaded area in Fig. 4a–d, referring to the frequent-NPF period in this study). However, this was not the case before June 29 and after July 6. Quantitatively, the model performed

https://doi.org/10.5194/egusphere-2023-540
Preprint. Discussion started: 23 August 2023

reasonably well in simulating SO_4^{2-} (MFB = 7 %, MFE = 54 % in Fig. 4e) and organics (MFB = -1 %, MFE = 40 % in Fig. 4h) with R = 0.52 and 0.58, respectively, during the frequent-NPF period. On July 5, the model mistakenly predicted the daytime wind direction to be mainly from the northeast, while the on-site recorded wind direction swayed between the southwest and the northwest. When excluding the evidently overestimated concentrations of $PM_{2.5}$ and all ions on July 5, the model performed better in reproducing SO_4^{2-} and organics. The MFB and MFE were below the goal values (i.e., MFB ⩽ 30 % and MFE ⩽ 50 %), and the R largely increased. For the modeled NH_4^+, the MFB and MFE met the benchmarks during the frequent-NPF period (Fig. 4g). Excluding the data on July 5 only slightly increased R. On the other hand, for the modeled NO_3^-, the model largely overestimated the observations, and the MFB (-125 %) and MFE (178 %) did not meet the benchmarks during the frequent-NPF period (Fig. 4f). Excluding the data on July 5, the model performed even worse in predicting NO_3^-. The simulations of NO_3^- in literature also showed a significant overestimate (Zakoura and Pandis, 2018; Travis et al., 2022).

The model demonstrated reasonable accuracy in reproducing $PM_{2.5}$ mass concentrations in both Beijing downtown (R = 0.49, MFB = 1 %, MFE = 49 %, as shown in Fig. 5c) and Beijing suburb (R = 0.42, MFB = -32 %, MFE = 69 %, as shown in Fig. 5d) during the frequent-NPF period (unshaded area in Fig. 5a–b). Notably, the model also performed well in simulating $PM_{2.5}$ mass concentrations prior to June 29, with an R value of 0.58 as well as MFB and MFE values of -14 % and 26 %, respectively, in Beijing downtown, and an R value of 0.54 as well as MFB and MFE values of -11 % and 33 %, respectively, in Beijing suburb. Overall, the model demonstrated reasonable accuracy in simulating the interested variables during June 29–July 6, except for NO_3^-. As such, we will focus our result analysis and discussion on the frequent-NPF period of good simulation performance.

3 Results and discussion

3.1 Overview of modeling NPF events

From June 29 to July 6, 2019, there were five NPF events, with the events being most frequently observed on June 29 and 30, July 1, July 3, and July 6, as shown in Fig. 6a–b. The high occurrence frequency of NPF events was associated with clean air masses from the north, and was favored by dry and sunny meteorological conditions, which is consistent with previous literature (Wu et al., 2007; Chu et al., 2021; Ma et al., 2021). During the NPF events on July 1 and 3, a typical banana-shaped growth pattern was observed, with the maximum median mode diameter of newly formed particles reaching over 60 nm and around 50 nm, respectively. The NPF events on June 29 and 30 also experienced rapid new particle growth during the initial 2–3 hours, but the maximum median mode diameters of the newly formed particles were smaller than 30 nm due to grown new particle shrinkage. Similarly, during the NPF event on July 6, the maximum median mode diameter of the newly formed particles was smaller than 30 nm before the new particle signal disappeared.

The modeling results effectively captured the occurrence characteristics of five NPF events, including their initial occurrence time and duration. Moreover, the model partially captured the growth

https://doi.org/10.5194/egusphere-2023-540
Preprint. Discussion started: 23 August 2023

characteristics of newly formed particles. However, the model failed to predict the shrinkage of newly formed particles on June 29 and 30, as no particle shrinkage mechanisms were included in the model. This was because particle shrinkage mechanisms were poorly understood (Yao et al., 2010; Skrabalova et al., 2015; Alonso-Blanco et al., 2017; Kamra et al., 2022). Furthermore, the modeling results reasonably reproduced the plumes of PNC occurring at nighttime on July 2 and 4, respectively. However, the model overestimated PNC plumes on July 5, which was consistent with the overestimation of $PM_{2.5}$, SO_4^{2-}, NO_3^-, NH_4^+, and organics, as mentioned above. This overestimation of PNC was previously reported by Matsui et al. (2011) who argued that it was due to the underestimation of vertical mixing capacity at night and excessive ground chemical concentrations in modeling. The similar arguments were also reported by Mckeen et al. (2007) and Matsui et al. (2009).

When considering NPF and non-NPF days separately, the simulated N_{ccn} at SS = 0.2 % met the goal values on non-NPF days, with MFB = 19 % and MFE = 48 % (Fig. 7a). However, on NPF days, the model substantially underestimated N_{ccn} at SS = 0.2 % (Fig. 7b). At SS = 0.4 %, the model reasonably reproduced the N_{ccn} on NPF days, with MFB = -46 % and MFE = 74 % (Fig. 7d). However, it substantially overestimated the N_{ccn} at SS = 0.4 % relative to the observations on non-NPF days (Fig. 7c). The underestimation or overestimation was determined not only by the estimated PNC with sizes larger than 60–120 nm but also by the Kappa values. We will delve into this further later on.

Based on the successful prediction of NPF events from June 29 to July 6 by the model, a comprehensive analysis of three distinct NPF events will be conducted in section 3.2–3.5. This analysis will include a detailed examination of the chemical drivers at ground level and their vertical profiles, the 3-D growth patterns of newly formed particles, the contributions of grown new particles to CCN, and other relevant factors.

3.2 Chemical drivers to grow newly formed particles and subsequently contribute to CCN at the ground level

Figure 8a–d present time series data for modeled chemical components of particles within two size ranges (10–40 nm and 40–250 nm) on July 1–2. During daytime, organics (ORG) were found to be the dominant contributor to growth in 10–40 nm particles, followed by $(NH_4)_2SO_4$. In contrast, NH_4NO_3 was the most significant chemical component driving growth in 40–250 nm particles during nighttime. To determine the relative contribution of each species as examples, their fractions in particles within each size range were calculated at two time points: 15:00 on July 1 (Fig. 8e–f) and 03:00 on July 2 (Fig. 8g–h). To account for differences in the contributions of secondary organics (SOA) and primary organics (POA) to new particle growth in the modeling results, SOA and POA were analyzed separately. In this study, SOA was defined as the sum of secondarily generated particulate organics from anthropogenic and biogenic precursors, while POA was the sum of primary organics.

At 15:00, the simulated SOA contributed to 56 % of the total mass of particles ranging from 10–40 nm, while $(NH_4)_2SO_4$ accounted for 36 %, and POA made up 8 % of the mass. The high mass fraction of $(NH_4)_2SO_4$ in 10–40 nm particles at 15:00 resulted in corresponding high hygroscopicity parameters (κ) of up to 0.24. The model predicted that the fraction of $(NH_4)_2SO_4$ in 40–250 nm particles was larger than that in 10–40 nm particles at 15:00, with $(NH_4)_2SO_4$ contributing to 49 % of the mass, followed by 44 %

https://doi.org/10.5194/egusphere-2023-540
Preprint. Discussion started: 23 August 2023

for SOA and 7 % for POA. This resulted in a corresponding κ value of up to 0.30. However, the estimated κ values based on observations at SS=1.0 %, 0.4 %, and 0.2 % were only 0.08, 0.08, and 0.16, respectively, at the same time, as reported in the companion paper. At 08:00, the model predicted that the concentration of H_2SO_4 vapor was approximately 10^8 molecules cm^{-3} (Fig. S1), which was substantially higher than previous observations in Beijing, where the maximum concentration was around 10^7 molecules cm^{-3} (Wang et al., 2011; Lu et al., 2019). Other modeling studies (Matsui et al., 2011; 2013) have also reported an overestimation of H_2SO_4 vapor similar to ours. In addition, gas-particle condensation has overwhelmingly contributed to POA in 10–40 nm particles, which also aided in the growth of newly formed particles. According to our simulated mass fractions of 40–250 nm particles (68% in $(NH_4NO_3+(NH_4)_2SO_4)$, 25 % in SOA, and 7 % in POA), the model-based κ value was estimated to be 0.37. However, at 03:00 on July 2, the observation-based estimated κ values at SS=1.0 %, 0.4 %, and 0.2 % were 0.10, 0.13, and 0.28, respectively, as reported in our companion paper. In this case, overestimation of NH_4NO_3 is likely to have contributed to the overestimation of κ values (Fig. 4b–c).

Similar to the NPF event on July 1–2, the modeling results on July 3–4 indicated that SOA was the dominant driver of new particle growth. Overestimation of H_2SO_4 vapor during the daytime resulted in overestimated κ values for particles ranging from 10–40 nm and 40–250 nm (Fig. S2 a–h). However, the model did not predict the formation of NH_4NO_3 before 24:00 on July 3, which was consistent with observation-based estimated κ values of less than 0.1 at SS levels of 0.4 % or higher.

On July 6, the model predicted that new particle growth was dominantly driven by SOA, with higher contributions than those observed on July 1–2 and July 3 (Fig. 9 a–j). Unlike the cases on July 1–2 and July 3, the κ values derived from the modeled mass fractions of 10–40 nm and 40–250 nm particles were reasonably consistent with the observation-based κ values on July 6. This suggests that there was no detectable evidence for overestimated H_2SO_4 vapor condensation during daytime on July 6. Additionally, the model did not predict the formation of NH_4NO_3 before 24:00 at nighttime.

Figure 10a–f displays the CCN simulation under 0.2 % and 0.4 % SS of NPF events on July 1, 3, and 6, respectively. During the NPF events, the N_{ccn} at 0.2 % SS were clearly underestimated by several folds. This underestimation was mainly due to the underestimates of number concentrations of preexisting particles >100 nm, as the κ values of particles at different sizes during the NPF events had been overestimated to some extent. However, the model reasonably reproduced N_{ccn} at 0.4 % SS during the NPF events on July 1 and 3. In these cases, the overestimation of number concentrations of grown new particles and their κ values probably canceled out the effect of the underestimated preexisting particles (>100 nm). However, this was not the case for the NPF event on July 6, when the grown new particles were too small to be activated as CCN. On that day, the N_{ccn} at 0.2 % SS were still underestimated to some extent.

3.3 Chemical drivers to grow newly formed particles in vertical direction

Based on the fact that the model reasonably reproduced $CN_{10–40}$ and organic drivers that lead to the growth of newly formed particles at the ground level, this section delves deeper into the chemical drivers at different heights during three selected NPF events. Figure 11a–d show the simulated chemical composition of 10–40 nm particles at three different heights (500 m, 1500 m, and 2500 m) over the

https://doi.org/10.5194/egusphere-2023-540
Preprint. Discussion started: 23 August 2023

observation site. These heights represent the lower part of the planetary boundary layer (PBL), the upper part of the PBL in the morning during the initial occurrence of NPF, and the top of the diurnal peak PBL on July 1–2, respectively. The results indicate that SOA dominated the growth of 10–40 nm particles at 500 m and 1500 m at 10:00, 15:00, and 22:00 on July 1. In contrast, inorganic species were found to steer growth at 2500 m during the same time, i.e., the ammoniated sulfuric acid likely acted as the dominant driver at 10:00, while the dominant driver switched to NH_4NO_3 at other times. This height-dependence of chemical drivers is consistent with previous findings in the literature, which attribute it to the low abundance of volatile organic compounds in the free troposphere (Sanchez et al., 2018; Williamson et al., 2019). On July 2 at 03:00, NH_4NO_3 acted as the dominant driver at all heights. However, as mentioned earlier, the ammoniated sulfuric acid and NH_4NO_3 in 10–40 nm particles may have been overestimated to some extent during daytime and nighttime, respectively, at the ground level. The same overestimation could also occur at different heights, underscoring the urgent need for vertical observations of chemical composition in 10–40 nm particles.

On July 3, the simulation showed a similar height-dependence of chemical drivers for the growth of newly formed particles (see Fig. S3). However, the model did not predict any NH_4NO_3 at a height of 500 m before the new particle signal disappeared. On July 6, the model predicted that a combination of SOA and POA contributed to approximately 80–90 % of the CN_{10-40} mass concentration at a height of 500 m during the event, as shown in Fig. 12. However, these percentages decreased with increasing height, dropping to approximately 35–60 % at a height of 2500 m. This indicates that inorganic species also played a significant role in the growth of newly formed particles, with an even contribution at higher altitudes.

3.4 3-D occurrence of NPF events and transport of newly formed particles

To investigate the 3-D occurrence of NPF events, we utilized the CN_{10} (summed number concentrations of particles with a diameter less than 10 nm) instead of CN_{10-40}. The simulated 3-D evolution of CN_{10} on July 1 is presented in Fig. 13a–b. The maximum CN_{10} value of approximately 8,000 cm^{-3} was predicted over the mountain station at around 1300 m above sea level, starting from 08:00 on July 1. At this point, the PBL had risen to approximately 1260 m above sea level. As reported in the literature, NPF events tend to occur initially in the residual layer due to high oxidation capacity, low condensation sink, and abundant precursors (Stratmann et al., 2003; Wehner et al., 2010; Quan et al., 2017; Qi et al., 2019; Tröstl et al., 2016). From 08:00 to 09:00 on July 1, NPF rapidly extended to the ground level, leading to a sharp increase in CN_{10} at that altitude (Fig. 13b). The NPF event reached its maximum concentration at the ground level between 10:00–11:00 and subsequently weakened.

When examining the occurrence of NPF in the horizontal direction at an altitude of approximately 1300 m a.s.l., a significant spatial inhomogeneity was predicted across the NCP. Specifically, the simulated CN_{10} revealed the presence of two stronger NPF regions located roughly 100–300 km away from the observational site at 08:00 (see Fig. 13a). From 09:00 to 12:00, these two stronger regions continued to expand and eventually connected with each other, forming a large zone approximately 270 km×135 km in size, located at 40.5–43 ºN and 115–116.5 ºE. When comparing the vertical distributions of the mountain station and point A, B (which represent the high-value areas of the two strong NPF

https://doi.org/10.5194/egusphere-2023-540
Preprint. Discussion started: 23 August 2023

regions) from 10:00 to 12:00, it was found that the simulated CN_{10} across the stronger NPF zone were approximately 3–4 times larger than those observed over most of the weaker NPF zones. However, the simulation also showed that there was no time lag for the occurrence of NPF, whether it was at the priority nucleation height of approximately 1300 m a.s.l. or on the ground over the NCP, as shown in Fig. 13a.

Similar to the event on July 1, NPF also occurred widely over the NCP on July 3. However, the stronger NPF zone was situated far away from the observational site (refer to Fig. S4). On July 6, NPF occurred over most parts of the NCP, as shown in Fig. S5. However, the areas of NPF occurrence were noticeably smaller compared to those on July 1 and 3, which could explain the shorter duration of NPF observed on July 6. Furthermore, the stronger NPF zone was located north of the observation site, and the strong northeast wind blew the new particle signal away from the observational site in the afternoon

3.5 What happened for grown new particles after their signals disappearing from observations?

The total number concentration of particles with sizes between 40 and 250 nm ($CN_{40–250}$) was used to characterize newly formed particles that had grown to a size where their signals were no longer observable. Figure 14a–b depicts the horizontal distribution of $CN_{40–250}$ at ground level from 18:00 on July 1 to 07:00 on July 2 and the corresponding vertical profiles of $CN_{40–250}$ over the observational zone and two stronger NPF zones. The simulated wind direction over the observational zone changed from northwest to southwest at 18:00 on July 1, coinciding with the decrease in observed new particle signals (as shown in Fig. 6a and Fig. 14a), due to weaker NPF events in the southwest direction. At that time, strong plumes were predicted in the southwest direction over a large area. By 24:00 on July 1, the modeling results indicated that these plumes had approached the observational zone. This intrusion likely led to an increase in both simulated and observed $CN_{40–250}$ from 24:00 on July 1 to 04:00 on July 2 (as shown in Fig. 6a), with the plume signal eventually overwhelming the new particle signal. The modeling results suggested that the new particle signal was converted to the signal of preexisting particles since then. Consequently, the question of whether grown new particles can experience additional growth to reach the CCN-required size was replaced by a new question: whether <20–50 nm preexisting particles, mainly composed of organics, can grow to the CCN-required size. In this study, preexisting particle growth only occurred on July 5, as presented in the companion paper. Unfortunately, the model poorly reproduced the observations on July 5. However, the occurrence frequency of preexisting particle growth was much less than that of NPF events.

Similar to what occurred on July 1, the new particle signal was also significantly diluted by the normal ambient signal, and by July 3, the signal had vanished from observations (see Fig. S6). However, this was not the case on July 6, as demonstrated in Fig. 15a–b. On that day, the strong northeast wind carried the new particle signal out of the observational zone, rather than diluting it into the normal ambient signal. It is still expected that the new particle signal will eventually be diluted into the ambient signal. Nevertheless, the modeling results need to be confirmed with Lagrange observations that track moving air masses.

4. Conclusion and uncertainties

https://doi.org/10.5194/egusphere-2023-540
Preprint. Discussion started: 23 August 2023

We used a 20-bin WRF-Chem model to simulate NPF events in the NCP during a three-week observational period in the summer of 2019. The model was able to reproduce the observations during June 29–July 6, which was characterized by a high frequency of NPF occurrence. Specifically, the model reasonably reproduced $CN_{10–40}$, N_{ccn} at 0.4 % SS, mass concentrations of $PM_{2.5}$, mass concentrations of SO_4^{2-} in $PM_{1.0}$ and TSP, ORG and NH_4^+ in $PM_{1.0}$, and other variables. However, the model consistently overestimated daytime H_2SO_4 vapor by approximately one order of magnitude and frequently overestimated nighttime formation of NH_4NO_3. These overestimations led to an overestimation of the κ values of both grown new particles and pre-existing particles to some extent. The model also poorly reproduced most of the observational variables during the remaining two weeks, and we have yet to explain this poor simulation. Our modeling results indicated that the growth of newly formed particles from 10 nm to larger sizes was overwhelmingly determined by SOA, which is consistent with previous modeling studies in the literature. This implies that the critical challenge in modeling NPF events may be accurately reproducing inorganic species rather than SOA.

The results of 3-D simulations of NPF events over the NCP, based on case studies, showed that NPF events occurred preferentially at the top of the PBL and then expanded vertically. In the horizontal direction, the NPF was predicted in a large regional scale with the stronger NPF zone located northeast of the observational site. The modeling results also suggested that SOA played a dominant role in steering the growth of newly formed particles in the PBL. However, inorganic species likely replaced SOA as the dominant driver above the PBL. Additional observations are needed to confirm these findings.

The model was able to reasonably reproduce the CCN at SS = 0.2 % on non-NPF days, but it clearly overestimated the CCN at SS = 0.4 % on those days. Conversely, the model was able to reasonably reproduce the CCN at SS = 0.4 % on NPF days, but it noticeably underestimated the CCN at SS = 0.2 %. This presents a significant challenge that must be urgently addressed, as it has a major impact on the accuracy of predicted contributions of NPF events to CCN budgets. Additionally, the disappearance of new particle signals in observations may simply be due to dilution effects or the movement of these signals elsewhere. In such cases, the issue of how newly formed particles grow into CCN becomes another important question: specifically, how do pre-existing particles with an organic-dominant composition of <20–50 nm grow into CCN?

Data availability. The data of this paper are available upon contact with the authors, Yang Gao (yanggao@ouc.edu.cn), Xiaohong Yao (xhyao@ouc.edu.cn) and Ming Chu (cm5594@stu.ouc.edu.cn).

Author contributions. YG and XY designed the experiments. MC conducted the experiments. MC, XW and SH analyzed the data, and MC wrote the paper. YG, XY, HG, YZ, BC, NM, JH and YS provided advice on data processing. YG and XY revised the original draft of the paper. All authors contributed to editing and improving the paper.

Competing interests. The authors declare that they have no conflict of interest.

https://doi.org/10.5194/egusphere-2023-540
Preprint. Discussion started: 23 August 2023

Acknowledgement. This research was supported by the National Natural Science Foundation of China (No. 42276036) and Hainan Provincial Natural Science Foundation of China (No. 422MS098). The simulations were conducted on Marine Big Data Center of Institute for Advanced Ocean Study of Ocean University of China. ChatGPT was used to polish the language paragraph-by-paragraph.

https://doi.org/10.5194/egusphere-2023-540
Preprint. Discussion started: 23 August 2023

References

Alonso-Blanco, E., Gómez-Moreno, F. J., Núñez, L., Pujadas, M., Cusack, M., and Artíñano, B.: Aerosol particle shrinkage event phenomenology in a South European suburban area during 2009–2015, Atmos. Environ., 160, 154-164, https://doi.org/10.1016/j.atmosenv.2017.04.013, 2017.

Bianchi, F., Tröstl, J., Junninen, H., Frege, C., Henne, S., Hoyle, C. R., Molteni, U., Herrmann, E., Adamov, A., Bukowiecki, N., Chen, X., Duplissy, J., Gysel, M., Hutterli, M., Kangasluoma, J., Kontkanen, J., Kürten, A., Manninen, H. E., Münch, S., Peräkylä, O., Petäjä, T., Rondo, L., Williamson, C., Weingartner, E., Curtius, J., Worsnop, D. R., Kulmala, M., Dommen, J., and Baltensperger, U.: New particle formation in the free troposphere: A question of chemistry and timing, Science, 352, 1109-1112, https://doi.org/10.1126/science.aad5456, 2016.

Bzdek, B. R. and Johnston, M. V.: New particle formation and growth in the troposphere, Anal. Chem., 82, 7871-7878, https://doi.org/10.1021/ac100856j, 2010.

Chen, X., Wang, Z., Li, J., and Yu, F.: Development of a Regional Chemical Transport Model with Size-Resolved Aerosol Microphysics and Its Application on Aerosol Number Concentration Simulation over China, Sola, 10, 83-87, https://doi.org/10.2151/sola.2014-017, 2014.

Chen, X., Wang, Z., Li, J., Chen, H., Hu, M., Yang, W., Wang, Z., Ge, B., and Wang, D.: Explaining the spatiotemporal variation of fine particle number concentrations over Beijing and surrounding areas in an air quality model with aerosol microphysics, Environ. Pollut., 231, 1302-1313, https://doi.org/10.1016/j.envpol.2017.08.103, 2017.

Chen, Z., Chen, D., Wen, W., Zhuang, Y., Kwan, M. P., Chen, B., Zhao, B., Yang, L., Gao, B., Li, R., and Xu, B.: Evaluating the "2+26" regional strategy for air quality improvement during two air pollution alerts in Beijing: variations in $PM_{2.5}$ concentrations, source apportionment, and the relative contribution of local emission and regional transport, Atmos. Chem. Phys., 19, 6879-6891, https://doi.org/10.5194/acp-19-6879-2019, 2019a.

Chen, X., Yang, W., Wang, Z., Li, J., Hu, M., An, J., Wu, Q., Wang, Z., Chen, H., Wei, Y., Du, H., and Wang, D.: Improving new particle formation simulation by coupling a volatility-basis set (VBS) organic aerosol module in NAQPMS+APM, Atmos. Environ., 204, 1-11, https://doi.org/10.1016/j.atmosenv.2019.01.053, 2019b.

Chow, J. C., Watson, J. G., Chen, L. W. A., Rice, J., and Frank, N. H.: Quantification of $PM_{2.5}$ organic carbon sampling artifacts in US networks, Atmos. Chem. Phys., 10, 5223-5239, https://doi.org/10.5194/acp-10-5223-2010, 2010.

Chu, B., Dada, L., Liu, Y., Yao, L., Wang, Y., Du, W., Cai, J., Dallenbach, K. R., Chen, X., Simonen, P., Zhou, Y., Deng, C., Fu, Y., Yin, R., Li, H., He, X. C., Feng, Z., Yan, C., Kangasluoma, J., Bianchi, F., Jiang, J., Kujansuu, J., Kerminen, V. M., Petaja, T., He, H., and Kulmala, M.: Particle growth with photochemical age from new particle formation to haze in the winter of Beijing, China, Sci. Total. Environ., 753, 142207, https://doi.org/10.1016/j.scitotenv.2020.142207, 2021.

Crippa, P. and Pryor, S. C.: Spatial and temporal scales of new particle formation events in eastern North America, Atmos. Environ., 75, 257-264, https://doi.org/10.1016/j.atmosenv.2013.04.051, 2013.

Cui, Y. Y., Hodzic, A., Smith, J. N., Ortega, J., Brioude, J., Matsui, H., Levin, E. J. T., Turnipseed, A., Winkler, P., and de Foy, B.: Modeling ultrafine particle growth at a pine forest site influenced by anthropogenic pollution during BEACHON-RoMBAS 2011, Atmos. Chem. Phys., 14, 11011-11029, https://doi.org/10.5194/acp-14-11011-2014, 2014.

Dai, L., Wang, H., Zhou, L., An, J., Tang, L., Lu, C., Yan, W., Liu, R., Kong, S., Chen, M., Lee, S., and Yu, H.: Regional and local new particle formation events observed in the Yangtze River Delta region,

https://doi.org/10.5194/egusphere-2023-540
Preprint. Discussion started: 23 August 2023

China, J. Geophys. Res., 122, 2389-2402, https://doi.org/10.1002/2016JD026030, 2017.

Dong, C., Matsui, H., Spak, S., Kalafut-Pettibone, A., and Stanier, C.: Impacts of New Particle Formation on Short-term Meteorology and Air Quality as Determined by the NPF-explicit WRF-Chem in the Midwestern United States, Aerosol Air Qual. Res., 19, 204-220, https://doi.org/10.4209/aaqr.2018.05.0163, 2019.

Dusek, U., Frank, G. P., Hildebrandt, L., Curtius, J., Schneider, J., Walter, S., Chand, D., Drewnick, F., Hings, S., Jung, D., Borrmann, S., and Andreae, M. O.: Size Matters More Than Chemistry for Cloud-Nucleating Ability of Aerosol Particles, Science, 312, 1375-1378, https://doi.org/10.1126/science.1125261, 2006.

Fast, J. D., Gustafson Jr, W. I., Easter, R. C., Zaveri, R. A., Barnard, J. C., Chapman, E. G., Grell, G. A., and Peckham, S. E.: Evolution of ozone, particulates, and aerosol direct radiative forcing in the vicinity of Houston using a fully coupled meteorology-chemistry-aerosol model, J. Geophys. Res., 111, https://doi.org/10.1029/2005JD006721, 2006.

Gordon, H., Kirkby, J., Baltensperger, U., Bianchi, F., Breitenlechner, M., Curtius, J., Dias, A., Dommen, J., Donahue, N. M., Dunne, E. M., Duplissy, J., Ehrhart, S., Flagan, R. C., Frege, C., Fuchs, C., Hansel, A., Hoyle, C. R., Kulmala, M., Kürten, A., Lehtipalo, K., Makhmutov, V., Molteni, U., Rissanen, M. P., Stozkhov, Y., Tröstl, J., Tsagkogeorgas, G., Wagner, R., Williamson, C., Wimmer, D., Winkler, P. M., Yan, C., and Carslaw, K. S.: Causes and importance of new particle formation in the present-day and preindustrial atmospheres, J. Geophys. Res., 122, 8739-8760, https://doi.org/10.1002/2017JD026844, 2017.

Grell, G. A., Peckham, S. E., Schmitz, R., McKeen, S. A., Frost, G., Skamarock, W. C., and Eder, B.: Fully coupled "online" chemistry within the WRF model, Atmos. Environ., 39, 6957-6975, https://doi.org/10.1016/j.atmosenv.2005.04.027, 2005.

Huang, X., Zhou, L., Ding, A., Qi, X., Nie, W., Wang, M., Chi, X., Petäjä, T., Kerminen, V.-M., Roldin, P., Rusanen, A., Kulmala, M., and Boy, M.: Comprehensive modelling study on observed new particle formation at the SORPES station in Nanjing, China, Atmos. Chem. Phys., 16, 2477-2492, https://doi.org/10.5194/acp-16-2477-2016, 2016.

Hudson, J. G.: Variability of the relationship between particle size and cloud-nucleating ability, Geophys. Res. Lett., 34, https://doi.org/10.1029/2006GL028850, 2007.

Hussein, T., Junninen, H., Tunved, P., Kristensson, A., Dal Maso, M., Riipinen, I., Aalto, P. P., Hansson, H. C., Swietlicki, E., and Kulmala, M.: Time span and spatial scale of regional new particle formation events over Finland and Southern Sweden, Atmos. Chem. Phys., 9, 4699-4716, https://doi.org/10.5194/acp-9-4699-2009, 2009.

Jiang, L. and Bai, L.: Spatio-temporal characteristics of urban air pollutions and their causal relationships: Evidence from Beijing and its neighboring cities, Sci. Rep., 8, 1279, https://doi.org/10.1038/s41598-017-18107-1, 2018.

Kamra, A. K., Victor, J. N., Siingh, D., Singh, A., and Dharmaraj, T.: Changes in the new particle formation and shrinkage events of the atmospheric ions during the COVID-19 lockdown, Urban. Clim., 44, 101214, https://doi.org/10.1016/j.uclim.2022.101214, 2022.

Kerminen, V. M., Chen, X. M., Vakkari, V., Petaja, T., Kulmala, M., and Bianchi, F.: Atmospheric new particle formation and growth: review of field observations, Environ. Res. Lett., 13, https://doi.org/10.1088/1748-9326/aadf3c, 2018.

Kim, Y., Kim, S.-W., Yoon, S.-C., Park, J.-S., Lim, J.-H., Hong, J., Lim, H.-C., Ryu, J., Lee, C.-K., and Heo, B.-H.: Characteristics of formation and growth of atmospheric nanoparticles observed at four

https://doi.org/10.5194/egusphere-2023-540
Preprint. Discussion started: 23 August 2023

regional background sites in Korea, Atmos. Res., 168, 80-91, https://doi.org/10.1016/j.atmosres.2015.08.020, 2016.

Kulmala, M., Vehkamäki, H., Petäjä, T., and Dal Maso, M.: Formation and growth rates of ultrafine atmospheric particles: a review of observations, J. Aerosol. Sci., 35, 143-176, https://doi.org/10.1016/j.jaerosci.2003.10.003, 2004.

Kulmala, M., Cai, R., Stolzenburg, D., Zhou, Y., Dada, L., Guo, Y., Yan, C., Petäjä, T., Jiang, J., and Kerminen, V.-M.: The contribution of new particle formation and subsequent growth to haze formation, Environ. Sci.: Atmos., 2, 352-361, https://doi.org/10.1039/D1EA00096A, 2022.

Lai, S. Y., Hai, S. F., Gao, Y., Wang, Y. H., Sheng, L. F., Lupascu, A., Ding, A. J., Nie, W., Qi, X. M., Huang, X., Chi, X. G., Zhao, C., Zhao, B., Shrivastava, M., Fast, J. D., Yao, X. H., and Gao, H. W.: The striking effect of vertical mixing in the planetary boundary layer on new particle formation in the Yangtze River Delta, Sci. Total. Environ., 829, https://doi.org/10.1016/j.scitotenv.2022.154607, 2022.

Li, S., Feng, K., and Li, M.: Identifying the main contributors of air pollution in Beijing, J. Clea. Prod., 163, S359-S365, https://doi.org/10.1016/j.jclepro.2015.10.127, 2017.

Lu, Y., Yan, C., Fu, Y., Chen, Y., Liu, Y., Yang, G., Wang, Y., Bianchi, F., Chu, B., Zhou, Y., Yin, R., Baalbaki, R., Garmash, O., Deng, C., Wang, W., Liu, Y., Petäjä, T., Kerminen, V. M., Jiang, J., Kulmala, M., and Wang, L.: A proxy for atmospheric daytime gaseous sulfuric acid concentration in urban Beijing, Atmos. Chem. Phys., 19, 1971-1983, https://doi.org/10.5194/acp-19-1971-2019, 2019.

Lupascu, A., Easter, R., Zaveri, R., Shrivastava, M., Pekour, M., Tomlinson, J., Yang, Q., Matsui, H., Hodzic, A., Zhang, Q., and Fast, J. D.: Modeling particle nucleation and growth over northern California during the 2010 CARES campaign, Atmos. Chem. Phys., 15, 12283-12313, https://doi.org/10.5194/acp-15-12283-2015, 2015.

Ma, L., Zhu, Y., Zheng, M., Sun, Y., Huang, L., Liu, X., Gao, Y., Shen, Y., Gao, H., and Yao, X.: Investigating three patterns of new particles growing to the size of cloud condensation nuclei in Beijing's urban atmosphere, Atmos. Chem. Phys., 21, 183-200, https://doi.org/10.5194/acp-21-183-2021, 2021.

Ma, M., Gao, Y., Wang, Y., Zhang, S., Leung, L. R., Liu, C., Wang, S., Zhao, B., Chang, X., Su, H., Zhang, T., Sheng, L., Yao, X., and Gao, H.: Substantial ozone enhancement over the North China Plain from increased biogenic emissions due to heat waves and land cover in summer 2017, Atmos. Chem. Phys., 19, 12195-12207, https://doi.org/10.5194/acp-19-12195-2019, 2019.

Man, H., Zhu, Y., Ji, F., Yao, X., Lau, N. T., Li, Y., Lee, B. P., and Chan, C. K.: Comparison of Daytime and Nighttime New Particle Growth at the HKUST Supersite in Hong Kong, Environ. Sci. Technol, 49, 7170-7178, https://doi.org/10.1021/acs.est.5b02143, 2015.

Matsui, H., Koike, M., Kondo, Y., Takegawa, N., Wiedensohler, A., Fast, J. D., and Zaveri, R. A.: Impact of new particle formation on the concentrations of aerosols and cloud condensation nuclei around Beijing, J. Geophys. Res., 116, https://doi.org/10.1029/2011jd016025, 2011.

Matsui, H., Koike, M., Kondo, Y., Takegawa, N., Kita, K., Miyazaki, Y., Hu, M., Chang, S. Y., Blake, D. R., and Fast, J. D. J. J. o. G. R. A.: Spatial and temporal variations of aerosols around Beijing in summer 2006: Model evaluation and source apportionment, J. Geophys. Res., https://doi.org/10.1029/2008jd010906, 2009.

Matsui, H., Koike, M., Takegawa, N., Kondo, Y., Takami, A., Takamura, T., Yoon, S., Kim, S. W., Lim, H. C., and Fast, J. D.: Spatial and temporal variations of new particle formation in East Asia using

https://doi.org/10.5194/egusphere-2023-540
Preprint. Discussion started: 23 August 2023

an NPF-explicit WRF-chem model: North-south contrast in new particle formation frequency, J. Geophys. Res., 118, 11,647-611,663, https://doi.org/10.1002/jgrd.50821, 2013.

Mckeen, S., Chung, S. H., Wilczak, J., Grell, G., Djalalova, I., Peckham, S., Gong, W., Bouchet, V., Moffet, R., and Tang, Y.: Evaluation of several $PM_{2.5}$ forecast models using data collected during the ICARTT/NEAQS 2004 field study, J. Geophys. Res., https://doi.org/10.1029/2006JD007608, 2007.

Merikanto, J., Spracklen, D. V., Mann, G. W., Pickering, S. J., and Carslaw, K. S.: Impact of nucleation on global CCN, Atmos. Chem. Phys., 9, 8601-8616, https://doi.org/10.5194/acp-9-8601-2009, 2009.

Metzger, A., Verheggen, B., Dommen, J., Duplissy, J., Prevot, A. S. H., Weingartner, E., Riipinen, I., Kulmala, M., Spracklen, D. V., Carslaw, K. S., and Baltensperger, U.: Evidence for the role of organics in aerosol particle formation under atmospheric conditions, Proc. Natl. Acad. Sci. U.S.A., 107, 6646-6651, https://doi.org/10.1073/pnas.0911330107, 2010.

Pikridas, M., Sciare, J., Freutel, F., Crumeyrolle, S., von der Weiden-Reinmuller, S. L., Borbon, A., Schwarzenboeck, A., Merkel, M., Crippa, M., Kostenidou, E., Psichoudaki, M., Hildebrandt, L., Engelhart, G. J., Petaja, T., Prevot, A. S. H., Drewnick, F., Baltensperger, U., Wiedensohler, A., Kulmala, M., Beekmann, M., and Pandis, S. N.: In situ formation and spatial variability of particle number concentration in a European megacity, Atmos. Chem. Phys., 15, 10219-10237, https://doi.org/10.5194/acp-15-10219-2015, 2015.

Qi, X., Ding, A., Nie, W., Chi, X., Huang, X., Xu, Z., Wang, T., Wang, Z., Wang, J., Sun, P., Zhang, Q., Huo, J., Wang, D., Bian, Q., Zhou, L., Zhang, Q., Ning, Z., Fei, D., Xiu, G., and Fu, Q.: Direct measurement of new particle formation based on tethered airship around the top of the planetary boundary layer in eastern China, Atmos. Environ., 209, 92-101, https://doi.org/10.1016/j.atmosenv.2019.04.024, 2019.

Quan, J., Liu, Y., Liu, Q., Jia, X., Li, X., Gao, Y., Ding, D., Li, J., and Wang, Z.: Anthropogenic pollution elevates the peak height of new particle formation from planetary boundary layer to lower free troposphere, Geophys. Res. Lett., 44, 7537-7543, https://doi.org/10.1002/2017GL074553, 2017.

Riccobono, F., Schobesberger, S., Scott, C. E., Dommen, J., Ortega, I. K., Rondo, L., Almeida, J., Amorim, A., Bianchi, F., Breitenlechner, M., David, A., Downard, A., Dunne, E. M., Duplissy, J., Ehrhart, S., Flagan, R. C., Franchin, A., Hansel, A., Junninen, H., Kajos, M., Keskinen, H., Kupc, A., Kürten, A., Kvashin, A. N., Laaksonen, A., Lehtipalo, K., Makhmutov, V., Mathot, S., Nieminen, T., Onnela, A., Petäjä, T., Praplan, A. P., Santos, F. D., Schallhart, S., Seinfeld, J. H., Sipilä, M., Spracklen, D. V., Stozhkov, Y., Stratmann, F., Tomé, A., Tsagkogeorgas, G., Vaattovaara, P., Viisanen, Y., Vrtala, A., Wagner, P. E., Weingartner, E., Wex, H., Wimmer, D., Carslaw, K. S., Curtius, J., Donahue, N. M., Kirkby, J., Kulmala, M., Worsnop, D. R., and Baltensperger, U.: Oxidation Products of Biogenic Emissions Contribute to Nucleation of Atmospheric Particles, Science, 344, 717-721, https://doi.org/10.1126/science.1243527, 2014.

Riipinen, I., Sihto, S.-L., Kulmala, M., Arnold, F., Dal Maso, M., Birmili, W., Kerminen, V.-M., Laaksonen, A., and Lehtinen, K. E. J.: Connections Between Ambient Sulphuric Acid and New Particle Formation in Hyytiälä and Heideleberg, Nucleation and Atmospheric Aerosols, Dordrecht, 2007, 1033-1037, https://doi.org/10.1007/978-1-4020-6475-3_205, 2007.

Sanchez, K. J., Chen, C.-L., Russell, L. M., Betha, R., Liu, J., Price, D. J., Massoli, P., Ziemba, L. D., Crosbie, E. C., Moore, R. H., Müller, M., Schiller, S. A., Wisthaler, A., Lee, A. K. Y., Quinn, P. K., Bates, T. S., Porter, J., Bell, T. G., Saltzman, E. S., Vaillancourt, R. D., and Behrenfeld, M. J.: Substantial Seasonal Contribution of Observed Biogenic Sulfate Particles to Cloud Condensation

https://doi.org/10.5194/egusphere-2023-540
Preprint. Discussion started: 23 August 2023

Nuclei, Sci. Rep., 8, 3235, https://doi.org/10.1038/s41598-018-21590-9, 2018.

Schobesberger, S., Junninen, H., Bianchi, F., Lönn, G., Ehn, M., Lehtipalo, K., Dommen, J., Ehrhart, S., Ortega, I. K., Franchin, A., Nieminen, T., Riccobono, F., Hutterli, M., Duplissy, J., Almeida, J., Amorim, A., Breitenlechner, M., Downard, A. J., Dunne, E. M., Flagan, R. C., Kajos, M., Keskinen, H., Kirkby, J., Kupc, A., Kürten, A., Kurtén, T., Laaksonen, A., Mathot, S., Onnela, A., Praplan, A. P., Rondo, L., Santos, F. D., Schallhart, S., Schnitzhofer, R., Sipilä, M., Tomé, A., Tsagkogeorgas, G., Vehkamäki, H., Wimmer, D., Baltensperger, U., Carslaw, K. S., Curtius, J., Hansel, A., Petäjä, T., Kulmala, M., Donahue, N. M., and Worsnop, D. R.: Molecular understanding of atmospheric particle formation from sulfuric acid and large oxidized organic molecules, Proc. Natl. Acad. Sci. U.S.A., 110, 17223-17228, https://doi.org/10.1073/pnas.1306973110, 2013.

Shen, X., Sun, J., Kivekäs, N., Kristensson, A., Zhang, X., Zhang, Y., Zhang, L., Fan, R., Qi, X., Ma, Q., and Zhou, H.: Spatial distribution and occurrence probability of regional new particle formation events in eastern China, Atmos. Chem. Phys., 18, 587-599, https://doi.org/10.5194/acp-18-587-2018, 2018.

Shen, Y., Meng, H., Yao, X., Peng, Z., Sun, Y., Zhang, J., Gao, Y., Feng, L., Liu, X., and Gao, H.: Does Ambient Secondary Conversion or the Prolonged Fast Conversion in Combustion Plumes Cause Severe $PM_{2.5}$ Air Pollution in China?, https://doi.org/10.3390/atmos13050673, 2022.

Sihto, S. L., Kulmala, M., Kerminen, V. M., Maso, M. D., Pet?J?, T., Riipinen, I., Korhonen, H., Arnold, F., Janson, R., Boy, M. J. A. C., and Physics: Atmospheric sulphuric acid and aerosol formation: implications from atmospheric measurements for nucleation and early growth mechanisms, Atmos. Chem. Phys., 6, 4079-4091, https://doi.org/10.5194/acp-6-4079-2006, 2006.

Skrabalova, L., Zikova, N., and Zdimal, V.: Shrinkage of Newly Formed Particles in an Urban Environment, Aerosol. Air. Qual. Res., 15, 1313-1324, https://doi.org/10.4209/aaqr.2015.01.0015, 2015.

Spracklen, D. V., Carslaw, K. S., Kulmala, M., Kerminen, V.-M., Sihto, S.-L., Riipinen, I., Merikanto, J., Mann, G. W., Chipperfield, M. P., Wiedensohler, A., Birmili, W., and Lihavainen, H.: Contribution of particle formation to global cloud condensation nuclei concentrations, Geophys. Res. Lett., 35, https://doi.org/10.1029/2007GL033038, 2008.

Stratmann, F., Siebert, H., Spindler, G., Wehner, B., Althausen, D., Heintzenberg, J., Hellmuth, O., Rinke, R., Schmieder, U., Seidel, C., Tuch, T., Uhrner, U., Wiedensohler, A., Wandinger, U., Wendisch, M., Schell, D., and Stohl, A.: New-particle formation events in a continental boundary layer: first results from the SATURN experiment, Atmos. Chem. Phys., 3, 1445-1459, https://doi.org/10.5194/acp-3-1445-2003, 2003.

Sullivan, R. C., Crippa, P., Matsui, H., Leung, L. R., Zhao, C., Thota, A., and Pryor, S. C.: New particle formation leads to cloud dimming, npj. Clim. Atmos. Sci., 1, 9, https://doi.org/10.1038/s41612-018-0019-7, 2018.

Travis, K. R., Crawford, J. H., Chen, G., Jordan, C. E., Nault, B. A., Kim, H., Jimenez, J. L., Campuzano-Jost, P., Dibb, J. E., Woo, J. H., Kim, Y., Zhai, S., Wang, X., McDuffie, E. E., Luo, G., Yu, F., Kim, S., Simpson, I. J., Blake, D. R., Chang, L., and Kim, M. J.: Limitations in representation of physical processes prevent successful simulation of $PM_{2.5}$ during KORUS-AQ, Atmos. Chem. Phys., 22, 7933-7958, https://doi.org/10.5194/acp-22-7933-2022, 2022.

Tröstl, J., Chuang, W. K., Gordon, H., Heinritzi, M., Yan, C., Molteni, U., Ahlm, L., Frege, C., Bianchi, F., Wagner, R., Simon, M., Lehtipalo, K., Williamson, C., Craven, J. S., Duplissy, J., Adamov, A., Almeida, J., Bernhammer, A.-K., Breitenlechner, M., Brilke, S., Dias, A., Ehrhart, S., Flagan, R. C.,

https://doi.org/10.5194/egusphere-2023-540
Preprint. Discussion started: 23 August 2023

Franchin, A., Fuchs, C., Guida, R., Gysel, M., Hansel, A., Hoyle, C. R., Jokinen, T., Junninen, H., Kangasluoma, J., Keskinen, H., Kim, J., Krapf, M., Kürten, A., Laaksonen, A., Lawler, M., Leiminger, M., Mathot, S., Möhler, O., Nieminen, T., Onnela, A., Petäjä, T., Piel, F. M., Miettinen, P., Rissanen, M. P., Rondo, L., Sarnela, N., Schobesberger, S., Sengupta, K., Sipilä, M., Smith, J. N., Steiner, G., Tomè, A., Virtanen, A., Wagner, A. C., Weingartner, E., Wimmer, D., Winkler, P. M., Ye, P., Carslaw, K. S., Curtius, J., Dommen, J., Kirkby, J., Kulmala, M., Riipinen, I., Worsnop, D. R., Donahue, N. M., and Baltensperger, U.: The role of low-volatility organic compounds in initial particle growth in the atmosphere, Nature, 533, 527-531, https://doi.org/10.1038/nature18271, 2016.

Wang, Z. B., Hu, M., Pei, X. Y., Zhang, R. Y., and Paasonen, P.: Connection of organics to atmospheric new particle formation and growth at an urban site of Beijing, Atmos. Environ., 103, 7-17, https://doi.org/10.1016/j.atmosenv.2014.11.069, 2015.

Wang, Z. B., Hu, M., Yue, D. L., Zheng, J., Zhang, R. Y., Wiedensohler, A., Wu, Z. J., Nieminen, T., and Boy, M.: Evaluation on the role of sulfuric acid in the mechanisms of new particle formation for Beijing case, Atmos. Chem. Phys., 11, 12663-12671, https://doi.org/10.5194/acp-11-12663-2011, 2011.

Wehner, B., Wiedensohler, A., Tuch, T. M., Wu, Z. J., Hu, M., Slanina, J., and Kiang, C. S.: Variability of the aerosol number size distribution in Beijing, China: New particle formation, dust storms, and high continental background, Geophys. Res. Lett., 31, https://doi.org/10.1029/2004GL021596, 2004.

Wehner, B., Siebert, H., Stratmann, F., Tuch, T., Wiedensohler, A., Petaja, T., Dal Maso, M., and Kulmala, M.: Horizontal homogeneity and vertical extent of new particle formation events, Tellus B: Chem. Phys. Meteorology., 59, 362-371, https://doi.org/10.1111/j.1600-0889.2007.00260.x, 2007.

Wehner, B., Siebert, H., Ansmann, A., Ditas, F., Seifert, P., Stratmann, F., Wiedensohler, A., Apituley, A., Shaw, R. A., Manninen, H. E., and Kulmala, M.: Observations of turbulence-induced new particle formation in the residual layer, Atmos. Chem. Phys., 10, 4319-4330, https://doi.org/10.5194/acp-10-4319-2010, 2010.

Wen, Z., Wang, C., Li, Q., Xu, W., Lu, L., Li, X., Tang, A., Collett, J. L., and Liu, X.: Winter air quality improvement in Beijing by clean air actions from 2014 to 2018, Atmos. Res., 259, 105674, https://doi.org/10.1016/j.atmosres.2021.105674, 2021.

Williamson, C. J., Kupc, A., Axisa, D., Bui, T., and Yu, P.: A large source of cloud condensation nuclei from new particle formation in the tropics, Nature, 574, 399, https://doi.org/10.1038/s41586-019-1638-9, 2019.

Wu, Z., Hu, M., Liu, S., Wehner, B., Bauer, S., Ma ßling, A., Wiedensohler, A., Petäjä, T., Dal Maso, M., and Kulmala, M.: New particle formation in Beijing, China: Statistical analysis of a 1-year data set, J. Geophys. Res. , 112, D09209, https://doi.org/10.1029/2006JD007406, 2007.

Yang, S., Li, X., Song, M., Liu, Y., Yu, X., Chen, S., Lu, S., Wang, W., Yang, Y., Zeng, L., and Zhang, Y.: Characteristics and sources of volatile organic compounds during pollution episodes and clean periods in the Beijing-Tianjin-Hebei region, Sci. Total. Environ., 799, 149491, https://doi.org/10.1016/j.scitotenv.2021.149491, 2021.

Yao, X., Lau, N. T., Fang, M., and Chan, C. K.: Real-Time Observation of the Transformation of Ultrafine Atmospheric Particle Modes, Aerosol. Sci. Tech., 39, 831-841, https://doi.org/10.1080/02786820500295248, 2005.

Yao, X., Choi, M. Y., Lau, N. T., Lau, A. P. S., Chan, C. K., and Fang, M.: Growth and Shrinkage of New Particles in the Atmosphere in Hong Kong, Aerosol. Sci. Tech., 44, 639-650,

https://doi.org/10.5194/egusphere-2023-540
Preprint. Discussion started: 23 August 2023

https://doi.org/10.1080/02786826.2010.482576, 2010.

Yao, X., Chan, C. K., Fang, M., Cadle, S., Chan, T., Mulawa, P., He, K., and Ye, B.: The water-soluble ionic composition of $PM_{2.5}$ in Shanghai and Beijing, China, Atmos. Environ., 36, 4223-4234, https://doi.org/10.1016/S1352-2310(02)00342-4, 2002.

Yao, X. H., Lau, N. T., Fang, M., and Chan, C. K.: On the time-averaging of ultrafine particle number size spectra in vehicular plumes, Atmos. Chem. Phys., 6, 4801-4807, https://doi.org/10.5194/acp-6-4801-2006, 2006.

Yu, F. and Hallar, A. G.: Difference in particle formation at a mountaintop location during spring and summer: Implications for the role of sulfuric acid and organics in nucleation, J. Geophys. Res. , 119, 12,246-212,255, https://doi.org/10.1002/2014JD022136, 2014.

Yu, F., Luo, G., Nadykto, A. B., and Herb, J.: Impact of temperature dependence on the possible contribution of organics to new particle formation in the atmosphere, Atmos. Chem. Phys., 17, 4997-5005, https://doi.org/10.5194/acp-17-4997-2017, 2017.

Yu, F. Q., Luo, G., Nair, A. A., Schwab, J. J., Sherman, J. P., and Zhang, Y. D.: Wintertime new particle formation and its contribution to cloud condensation nuclei in the Northeastern United States, Atmos. Chem. Phys., 20, 2591-2601, https://doi.org/10.5194/acp-20-2591-2020, 2020.

Yue, D. L., Hu, M., Zhang, R. Y., Wang, Z. B., Zheng, J., Wu, Z. J., Wiedensohler, A., He, L. Y., Huang, X. F., and Zhu, T.: The roles of sulfuric acid in new particle formation and growth in the mega-city of Beijing, Atmos. Chem. Phys., 10, 4953-4960, https://doi.org/10.5194/acp-10-4953-2010, 2010.

Zakoura, M. and Pandis, S. N.: Overprediction of aerosol nitrate by chemical transport models: The role of grid resolution, Atmos. Environ., 187, 390-400, https://doi.org/10.1016/j.atmosenv.2018.05.066, 2018.

Zhang, R., Khalizov, A., Wang, L., Hu, M., and Xu, W.: Nucleation and growth of nanoparticles in the atmosphere, Chem. Rev., 112, 1957-2011, https://doi.org/10.1021/cr2001756, 2012.

Zhang, W., Li, W., An, X., Zhao, Y., Sheng, L., Hai, S., Li, X., Wang, F., Zi, Z., and Chu, M.: Numerical study of the amplification effects of cold-front passage on air pollution over the North China Plain, Sci. Total. Environ., 833, 155231, https://doi.org/10.1016/j.scitotenv.2022.155231, 2022.

Zhou, Y., Dada, L., Liu, Y., Fu, Y., Kangasluoma, J., Chan, T., Yan, C., Chu, B., Daellenbach, K. R., Bianchi, F., Kokkonen, T. V., Liu, Y., Kujansuu, J., Kerminen, V. M., Petäjä, T., Wang, L., Jiang, J., and Kulmala, M.: Variation of size-segregated particle number concentrations in wintertime Beijing, Atmos. Chem. Phys., 20, 1201-1216, https://doi.org/10.5194/acp-20-1201-2020, 2020.

Zhu, Y., Yan, C., Zhang, R., Wang, Z., Zheng, M., Gao, H., Gao, Y., and Yao, X.: Simultaneous measurements of new particle formation at 1 s time resolution at a street site and a rooftop site, Atmos. Chem. Phys., 17, 9469-9484, https://doi.org/10.5194/acp-17-9469-2017, 2017.

Zhu, Y., Shen, Y., Li, K., Meng, H., Sun, Y., Yao, X., Gao, H., Xue, L., and Wang, W.: Investigation of Particle Number Concentrations and New Particle Formation With Largely Reduced Air Pollutant Emissions at a Coastal Semi-Urban Site in Northern China, J. Geophys. Res. Atmos., 126, e2021JD035419, https://doi.org/10.1029/2021JD035419, 2021a.

Zhu, Y., Xue, L., Gao, J., Chen, J., Li, H., Zhao, Y., Guo, Z., Chen, T., Wen, L., Zheng, P., Shan, Y., Wang, X., Wang, T., Yao, X., and Wang, W.: Increased new particle yields with largely decreased probability of survival to CCN size at the summit of Mt. Tai under reduced SO_2 emissions, Atmos. Chem. Phys., 21, 1305-1323, https://doi.org/10.5194/acp-21-1305-2021, 2021b.

https://doi.org/10.5194/egusphere-2023-540
Preprint. Discussion started: 23 August 2023

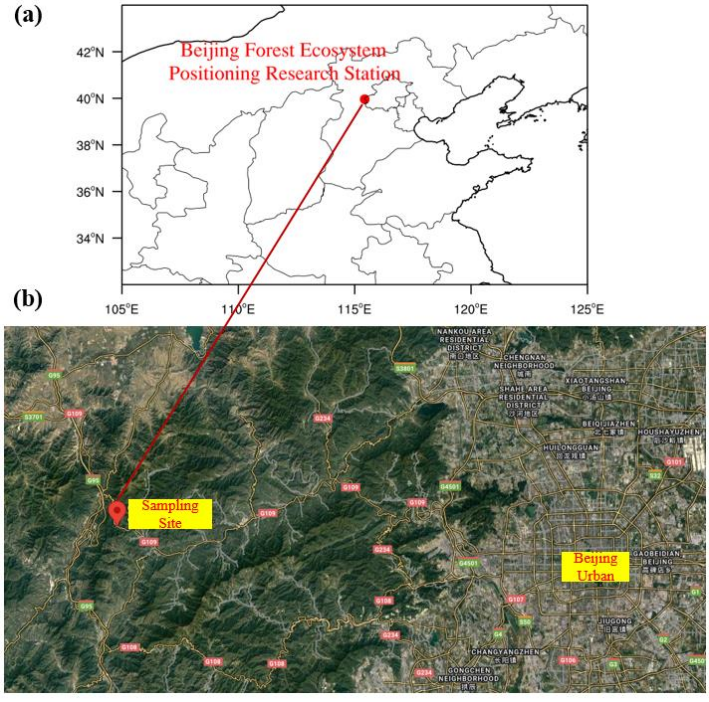

Figure 1. Map of sampling site (a) and 3-D view of sampling site (b) in summer © Google Maps (download from https://www.google.com/maps/).

https://doi.org/10.5194/egusphere-2023-540
Preprint. Discussion started: 23 August 2023

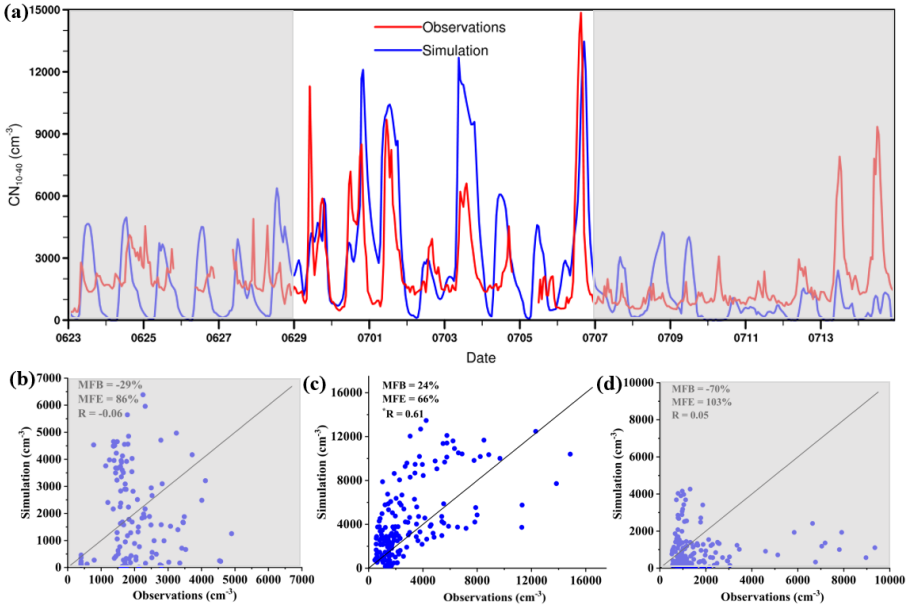

Figure 2. Time series of observed and modeled $CN_{10–40}$ from June 23 to July 14 (a), the comparison of the modeled $CN_{10–40}$ with the observations in June 23–28 (b), in June 29–July 6 (c) and in July 7–July 14 (d).

https://doi.org/10.5194/egusphere-2023-540
Preprint. Discussion started: 23 August 2023

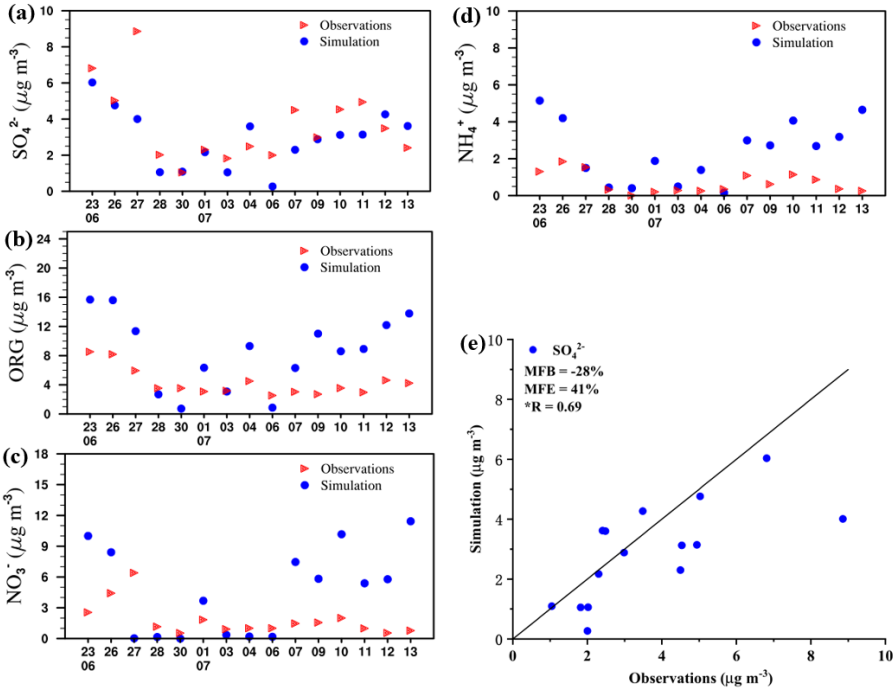

Figure 3. Time series of observed and modeled mass concentrations of SO_4^{2-} (a), organics (b), NO_3^- (c) and NH_4^+ (d) in June 23–July 14, and comparison of the modeled and observed SO_4^{2-}.

https://doi.org/10.5194/egusphere-2023-540
Preprint. Discussion started: 23 August 2023

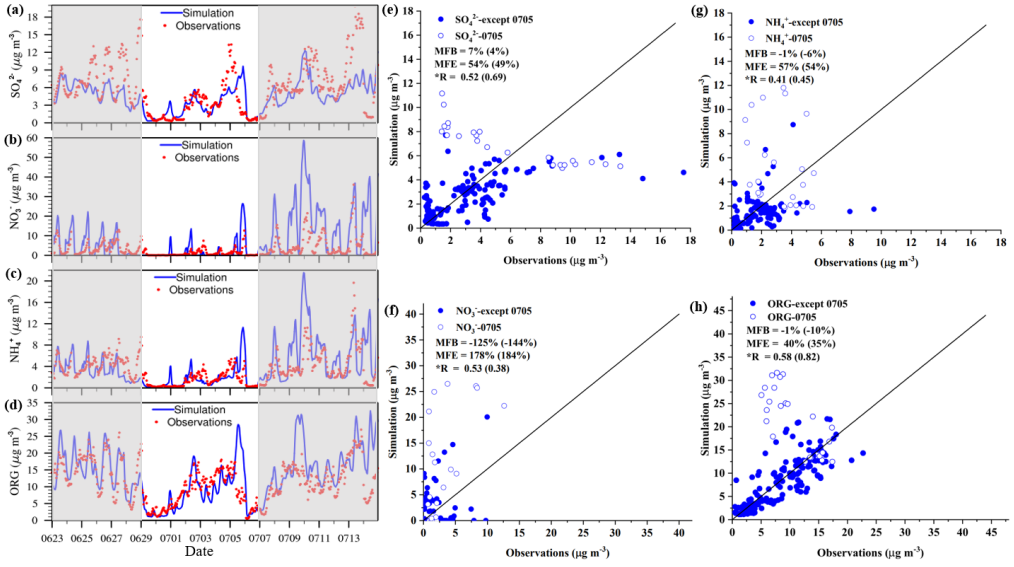

Figure 4. Time series of simulated and observed particle mass concentrations of SO_4^{2-} (a), NO_3^- (b), NH_4^+ (c) and organics (d) in $PM_{1.0}$ at an urban site (39.98°N, 116.39°E) in Beijing from June 23 to July 14 and the comparison between the simulated and observed SO_4^{2-} (e), NO_3^- (f), NH_4^+ (g) and organics (h) during the frequent-NPF period of June 29–July 6 (the MFB, MFE and R in parentheses are calculated with the data excluding July 5, empty symbols in e-h represent the data on July 5).

https://doi.org/10.5194/egusphere-2023-540
Preprint. Discussion started: 23 August 2023

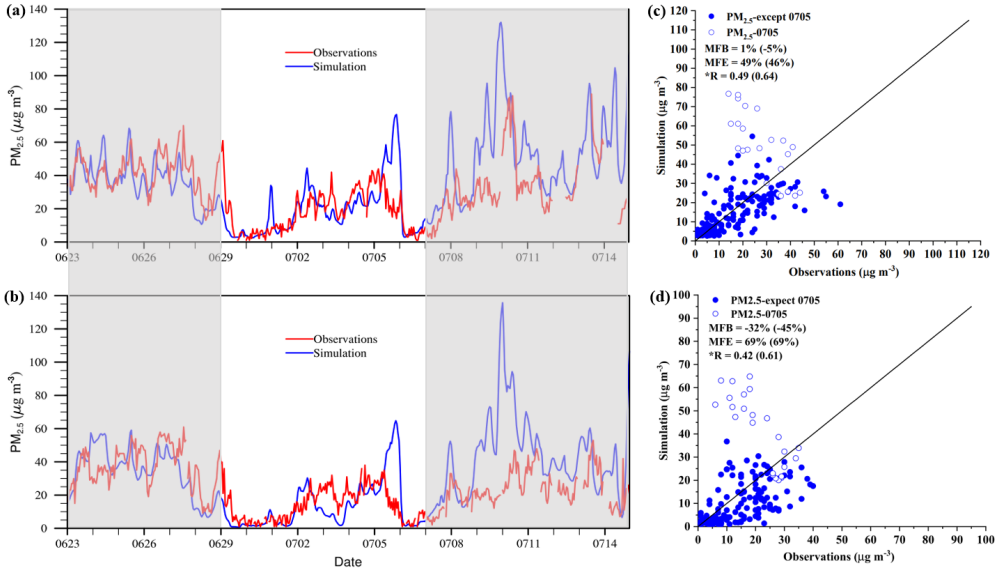

Figure 5. Time series of the observed and modeled $PM_{2.5}$ mass concentrations from June 23 to July 14 in Beijing downtown (a: 39.86°N, 116.36°E) and Beijing suburb (b: 40.19°N, 116.23°E), the comparison of the modeled and observed $PM_{2.5}$ during the frequent-NPF period in Beijing downtown (c) and Beijing suburb (d, the MFB, MFE and R in parentheses are calculated with the data excluding July 5).

https://doi.org/10.5194/egusphere-2023-540
Preprint. Discussion started: 23 August 2023

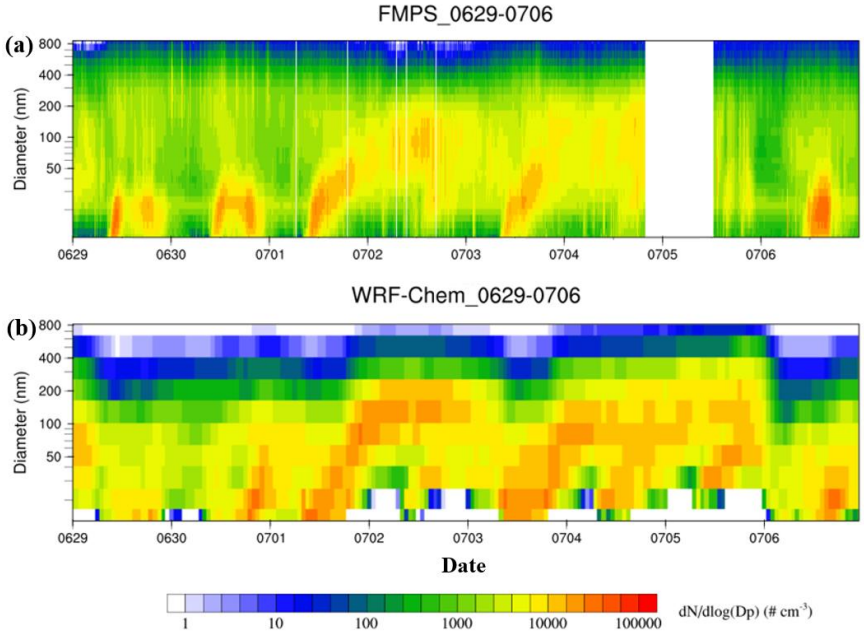

Figure 6. Contour plot of PNSDs from observations (a) and modeling (b) from June 29 to July 6, 2019.

https://doi.org/10.5194/egusphere-2023-540
Preprint. Discussion started: 23 August 2023

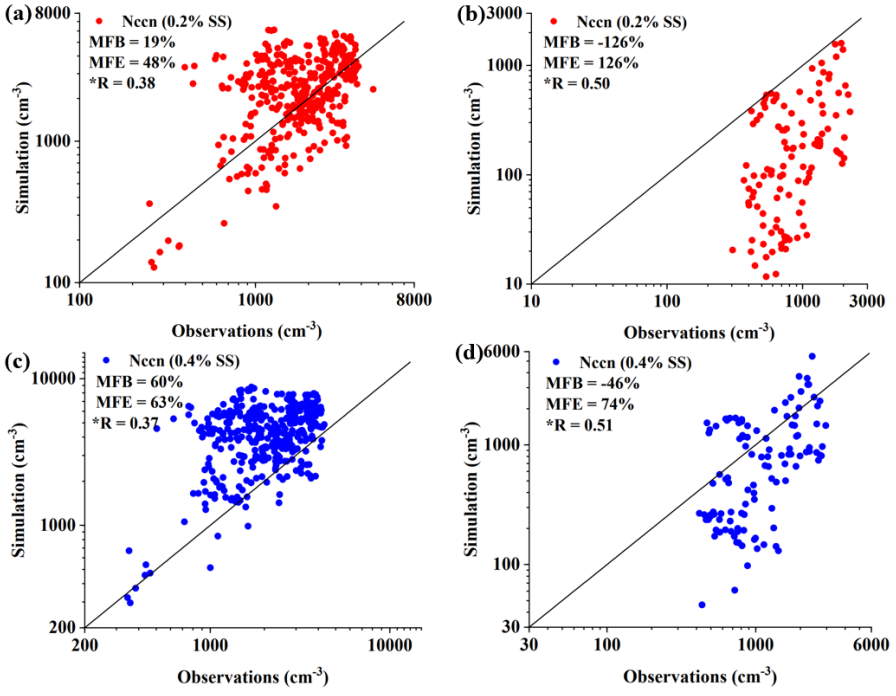

Figure 7. The simulated N_{ccn} against the observations at 0.2 % SS (a–b) and 0.4 % SS (c–d) on non-NPF days and NPF days, respectively, during the frequent-NPF period.

https://doi.org/10.5194/egusphere-2023-540
Preprint. Discussion started: 23 August 2023

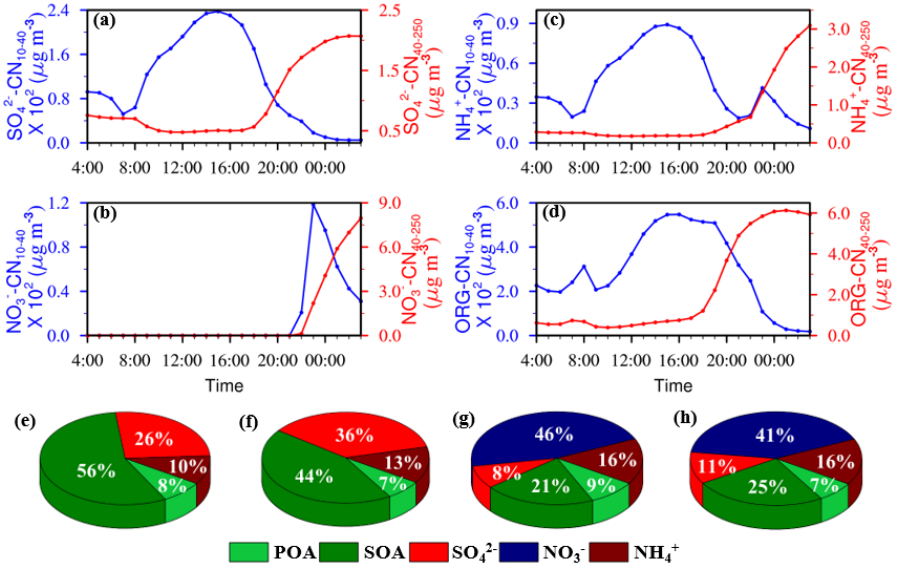

Figure 8. Diurnal variations in modeled chemical components in 10–40 nm particles and 40–250 nm particles: SO_4^{2-} (a), NO_3^- (b), NH_4^+ (c), organics (d) on July 1–2; fractions of chemical species in 10–40 nm particles (e) and 40-250 nm particles (f) at 15:00 on July 1 and those at 3:00 on July 2 (g and h).

https://doi.org/10.5194/egusphere-2023-540
Preprint. Discussion started: 23 August 2023

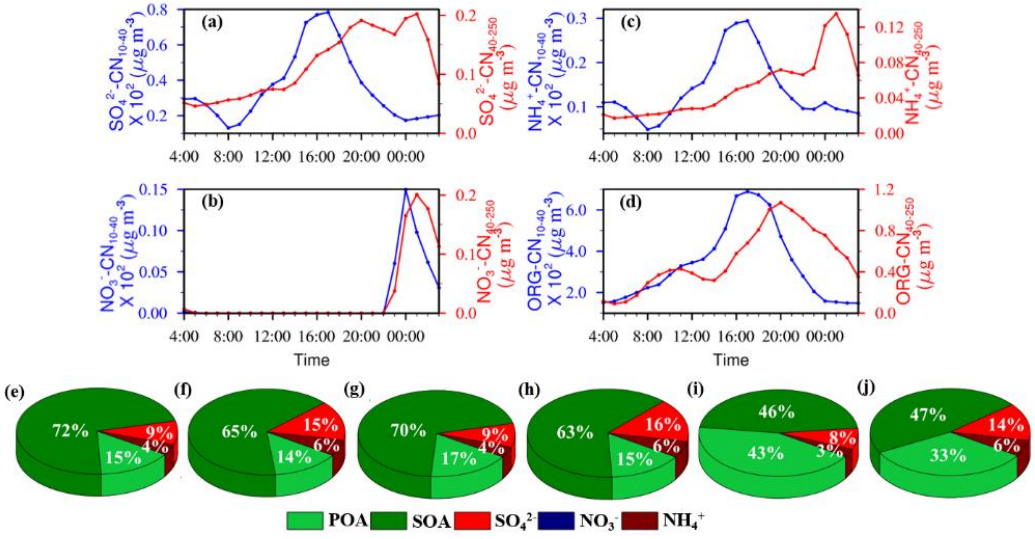

Figure 9. Diurnal variation in modeled chemical components in 10–40 nm particles and 40–250 nm particles: SO_4^{2-} (a), NO_3^- (b), NH_4^+ (c), organics (d) on July 6–7; fractions of chemical species in 10–40 nm particles (e) and 40–250 nm particles (f) at 12:00, those at 17:00 (g and h) and those at 22:00 on July 6 (i and j).

https://doi.org/10.5194/egusphere-2023-540
Preprint. Discussion started: 23 August 2023

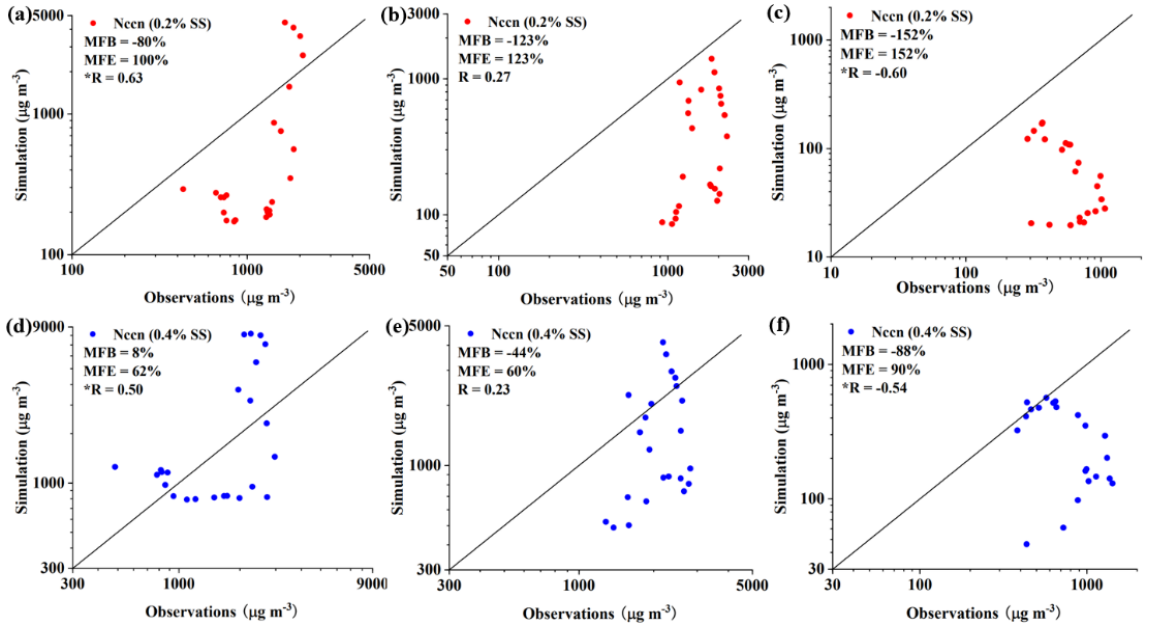

Figure 10. The simulations of CCN number concentration at 0.2 % SS (a–c) and 0.4 % SS (d–f) on the NPF events of July 1, 3, 6, respectively.

https://doi.org/10.5194/egusphere-2023-540
Preprint. Discussion started: 23 August 2023

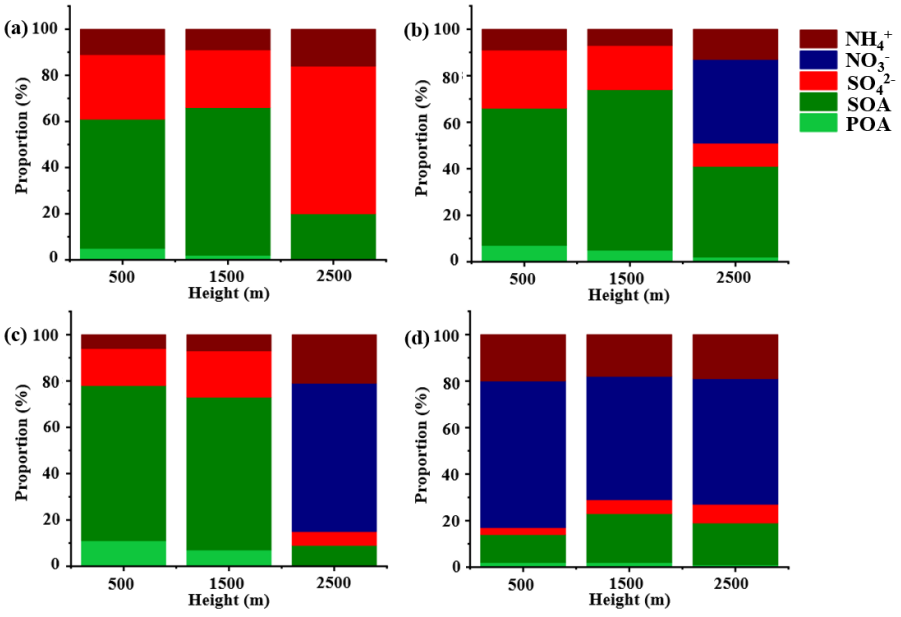

Figure 11. The simulated chemical components in 10–40 nm particles at 500 m, 1500 m and 2500 m above the ground respectively at 10:00 (a), 15:00 (b), 22:00 (c) on July 1 and 3:00 (d) on July 2.

https://doi.org/10.5194/egusphere-2023-540
Preprint. Discussion started: 23 August 2023

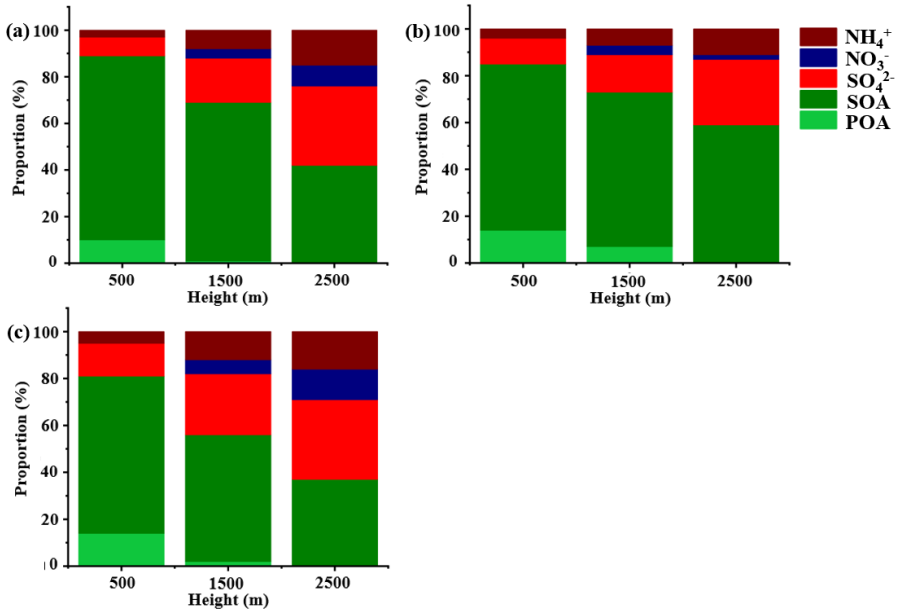

Figure 12. The simulated chemical components in 10–40 nm particles at 500 m, 1500 m and 2500 m above the ground respectively at 12:00 (a), 15:00 (b), 18:00 (c) on July 6.

https://doi.org/10.5194/egusphere-2023-540
Preprint. Discussion started: 23 August 2023

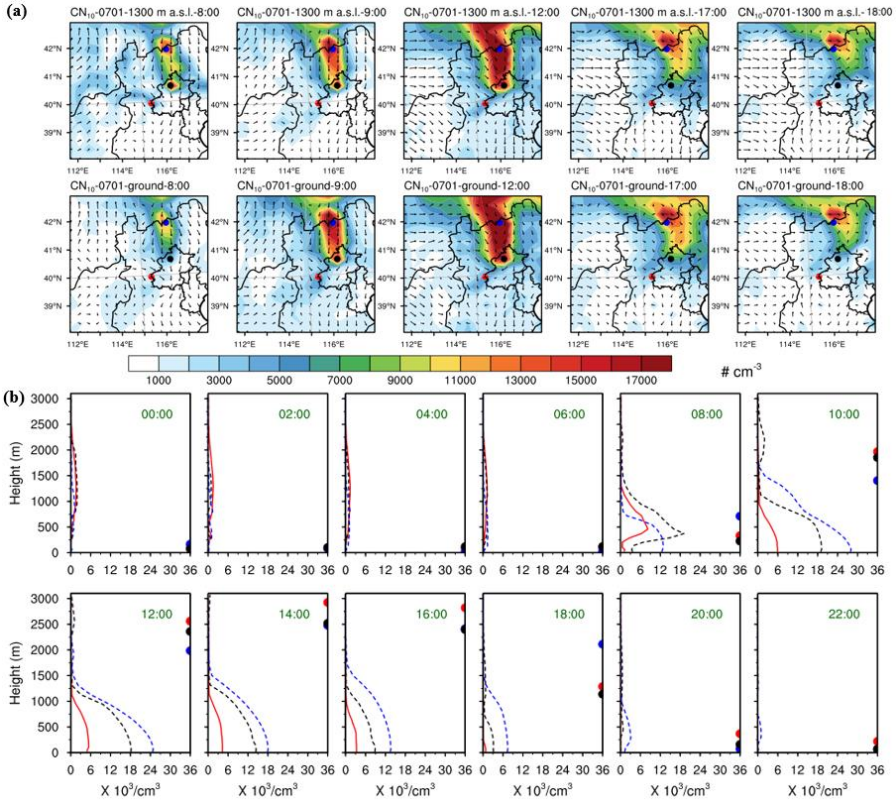

Figure 13. Horizontal distribution of CN_{10} at ~1300 m a.s.l. (a, the upper row) and on the ground level (a, the bottom row) at 8:00, 9:00, 12:00, 17:00 and 18:00 on July 1, 2019 (the red, blue and black solid dots represent the observation site, two centers of strong NPF zones (point A and point B), respectively; the direction and length of the black arrow represent the wind direction and wind speed, respectively); Vertical profiles of CN_{10} over the observational site (red solid line), point A (blue dashed line) and point B (black dashed line) from 0:00 to 22:00 on July 1, 2019 (b, the Y-axis coordinate is the height above the ground; the red, blue and black solid dots represent the height of the PBL over the observational site, point A and point B, and PBL exceeding 3000 meters above the ground are not shown in Figure).

https://doi.org/10.5194/egusphere-2023-540
Preprint. Discussion started: 23 August 2023

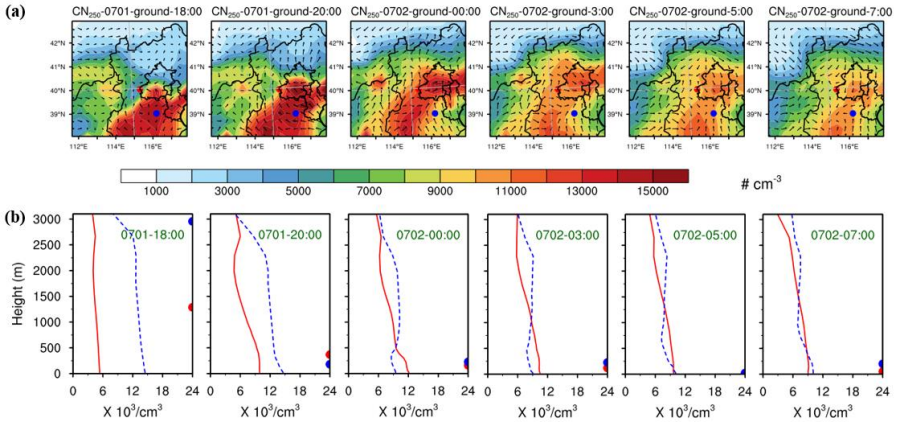

Figure 14. Horizontal distribution of CN_{40-250} on ground (a, the upper row) and vertical profiles of CN_{40-250} over the observational site (red solid line) and point A (blue dashed line) from 18:00 on July 1 to 07:00 on July 2 (b, the Y-axis coordinate is the height above the ground; the red and blue solid dots represent the height of the PBL over the observational site and point A, and PBL exceeding 3000 meters above the ground are not shown in Figure).

https://doi.org/10.5194/egusphere-2023-540
Preprint. Discussion started: 23 August 2023

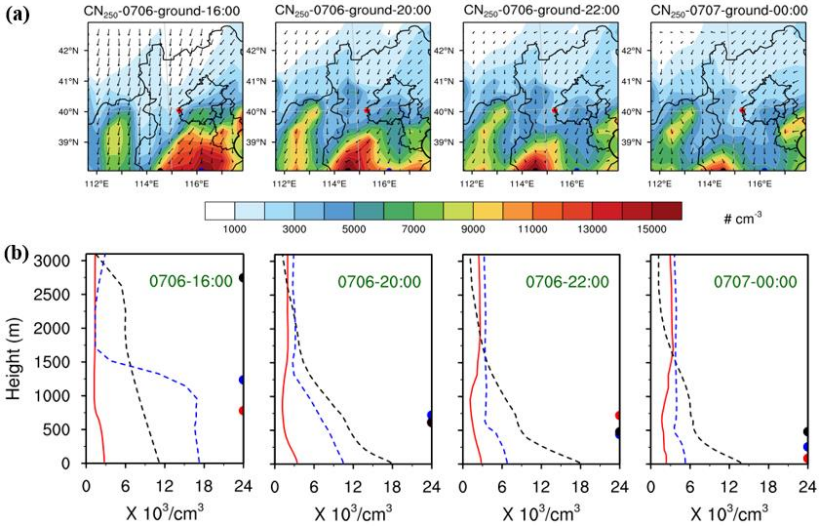

Figure 15. Horizontal distribution of CN_{40-250} on ground (a, the upper row) and vertical profile of CN_{40-250} in observation site (red solid line), point A (blue dashed line) and point B (black dashed line) in the NPF event occurred on July 6 from 16:00 on July 6 to 00:00 on July 7 (b, the Y-axis coordinate is the height above the ground; the red, blue and black solid dots represent the height of the PBL in observation site, point A and point B, and PBL exceeding 3000 meters above the ground are not shown in the figure).